

# Quasinormal modes and greybody factor of Schwarzschild

## Black Hole in the Cold Dark Matter Halo

Shi-Jie Ma, Rui-Bo Wang, Jian-Bo Deng,<sup>\*</sup> and Xian-Ru Hu<sup>†</sup>

*Lanzhou Center for Theoretical Physics,*

*Key Laboratory of Theoretical Physics of Gansu Province,*

*Lanzhou University, Lanzhou, Gansu 730000, China*

Tian-Chi Ma<sup>‡</sup>

*Center for Gravitational Physics, Department of Space Science,*

*Beihang University, Beijing 100191, China*

He-Xu Zhang<sup>§</sup>

*Center for Theoretical Physics and College of Physics,*

*Jilin University, Changchun, 130012, China*

## Abstract

In this article, we firstly studied wave function in static spherically symmetric spacetime and obtained effective potential of perturbed fields with spin. Then we applied 6<sup>th</sup> order WKB approximation to analyze quasinormal modes of Schwarzschild black hole in the Cold Dark Matter halo in perturbed fields with different spins and derived quasinormal frequencies. Further, to study the relation between quasinormal frequencies and optics, we compare the results of WKB method with eikonal limit formula. At last, we discussed greybody factor in different perturbed fields under this spacetime.

---

\* Email: [dengjb@lzu.edu.cn](mailto:dengjb@lzu.edu.cn)

† Email(corresponding author): [huxianru@lzu.edu.cn](mailto:huxianru@lzu.edu.cn)

‡ Email: [tianchima@buaa.edu.cn](mailto:tianchima@buaa.edu.cn)

§ Email: [hxzhang18@163.com](mailto:hxzhang18@163.com)

## I. INTRODUCTION

Many phenomena in cosmic research had been explained and predicted since Einstein established general relativity [1–4]. Recent observations have shown divergence from theoretical predictions. The prevailing view is that there is a large amount of dark matter in the universe (about 85%) [5–7]. This kind of matter can only engage in gravitational interaction, making it hard to be observed by normal method. This is why it is called “dark”.

Cold Dark Matter (CDM) is proposed in [8] and it have be verified that this dark matter model is consistent with observations of the large-scale structure of the universe. Since it was proposed, this model has been favored by cosmologists and has been widely studied. Particularly, the  $\Lambda$ CDM model is used by most cosmologists to describe the development of the universe [9, 10]. Modern cosmological models indicate that dark matter halos are the fundamental unit of cosmic structure. The current hypothesis for dark matter halo is based on CDM and its significant role in the early formation of galaxy. Black holes in the CDM halo have also been extensively studied in recent years [11–13].

Quasinormal mode (QNM) is a kind of gravitational wave produced by black hole mergers during the ringdown phase [14], with a complex characteristic frequency called “quasinormal frequency” (QNF). The real parts of the QNFs are the oscillation frequencies of the perturbation, and the imaginary parts are related to the decay time.

The QNMs of the gravitational field can only depend on the parameter of the black hole, so the study of QNMs can help us understand black holes more precisely [15–18]. This is why QNMs have attracted more interest of researchers in recent years. There are many method used to study the QNMs of black holes. The most commonly used method is the Wentzel-Kramers-Brillouin (WKB) approximative method [19–26]. In addition, the relationship between QNFs and black hole shadows could be linked by the eikonal limit formula [27–30].

In addition, greybody factor is also a significant concept for black hole spacetime with perturbed field. Greybody factor is used to describe the transmission probability of an outgoing wave reaching to infinity or an incoming wave to be absorbed by black hole [31–33]. The greybody factor is so important because it could effectively help to analyze the information behavior near horizon regions of a black hole [34]. And it could be used to estimate the energy emission of Hawking radiation [35]. Besides, it should be emphasized that it was suggested that greybody factor played a important role in the research on ringdown signal after an extreme mass ratio merger [36].

In this paper, we study the QNM and greybody factor of Schwarzschild black hole in the CDM halo. This article is organized as follows. In Sect. II, we discuss the wave equation of QNMs and the effective potential. In Sect. III, we use 6<sup>th</sup> order WKB method to study the QNFs and the influences of CDM halo. In Sect. IV, we compare the results of the WKB method with the eikonal limit formula. We also

have calculated the greybody factor of black holes in detail. In Sect. VI, we finally conclude our study. To simplify the calculation, we assume  $G_N = M = c = 1$ .

## II. PERTURBED FIELD AND EFFECTIVE POTENTIAL

For a static spherically symmetric black hole, its metric could be written as

$$ds^2 = -f(r) dt^2 + \frac{1}{f(r)} dr^2 + r^2 (d\theta^2 + \sin^2 \theta d\varphi^2). \quad (1)$$

With this background spacetime, a massless scalar field  $\Phi$  obeys the Klein-Gorden equation

$$\square\Phi \equiv \frac{1}{\sqrt{-g}} \partial_\mu (\sqrt{-g} g^{\mu\nu} \partial_\nu \Phi) = 0, \quad (2)$$

where  $g^{\mu\nu}$  is inverse metric,  $g$  is the determinant of metric  $g_{\mu\nu}$ , and  $\Phi$  is the wave function incoming from infinity towards the black hole.

As is done in quantum mechanics, the Klein-Gorden equation could be solved by separating the variables

$$\Phi(t, r, \theta, \phi) = \frac{e^{-i\omega t}}{r} \Psi(r) Y_\ell^m(\theta, \phi), \quad (3)$$

where  $\omega$  is the frequency of  $\Phi$ ,  $\Psi(r)$  is radial wave function.  $\ell$  is azimuthal quantum number, and takes only nonnegative integers.  $m$  is magnetic quantum number, and in this article we always choose it as zero.  $Y_\ell^m$  is spherical harmonic function, and it

fulfills the relations

$$\left[ \frac{1}{\sin \theta} \partial_\theta (\sin \theta \partial_\theta) + \frac{1}{\sin^2 \theta} \partial_\phi^2 \right] Y_\ell^m (\theta, \phi) = -\ell(\ell + 1) Y_\ell^m (\theta, \phi). \quad (4)$$

Inserting Eq. (3) into Eq. (2), the Regge-Wheeler wave equation [37] is obtained

$$\left[ \frac{\partial^2}{\partial t^2} - \frac{\partial^2}{\partial r_*^2} + V_{eff} (r) \right] \Psi (r) e^{-i\omega t} = 0, \quad (5)$$

which could also be written as

$$\frac{d^2}{dr_*^2} \Psi + (\omega^2 - V_{eff}) \Psi = 0, \quad (6)$$

with "tortoise" radial coordinate  $r_* = \int dr/f(r)$  and the effective potential  $V_{eff}$ .

For a massless scalar field,  $V_{eff}$  reads

$$V_{eff} (r) = f (r) \left[ \frac{\ell (\ell + 1)}{r^2} + \frac{1}{r} \frac{df (r)}{dr} \right]. \quad (7)$$

A generalized form of the effective potential for higher spin (boson) fields is given by [38, 39]

$$V_{eff} (r) = f (r) \left[ \frac{\ell (\ell + 1)}{r^2} + (s - s^2) \frac{1 - f (r)}{r^2} + (1 - s) \frac{1}{r} \frac{df (r)}{dr} \right], \quad (8)$$

where  $s \leq l$  is the spin of the perturbative field

$$s = \begin{cases} 0, & \text{scalar perturbation,} \\ 1, & \text{electromagnetic perturbation,} \\ 2, & \text{gravitational perturbation.} \end{cases} \quad (9)$$

In this paper, we study the QNM of Schwarzschild black hole in the CDM halo [11, 12]

$$f(r) = \left(1 + \frac{r}{R_0}\right)^{-\frac{8\pi\rho_0 R_0^3}{r}} - \frac{2}{r}, \quad (10)$$

where  $\rho_0$  is the density of the CDM halo collapse and  $R_0$  is the feature radius.

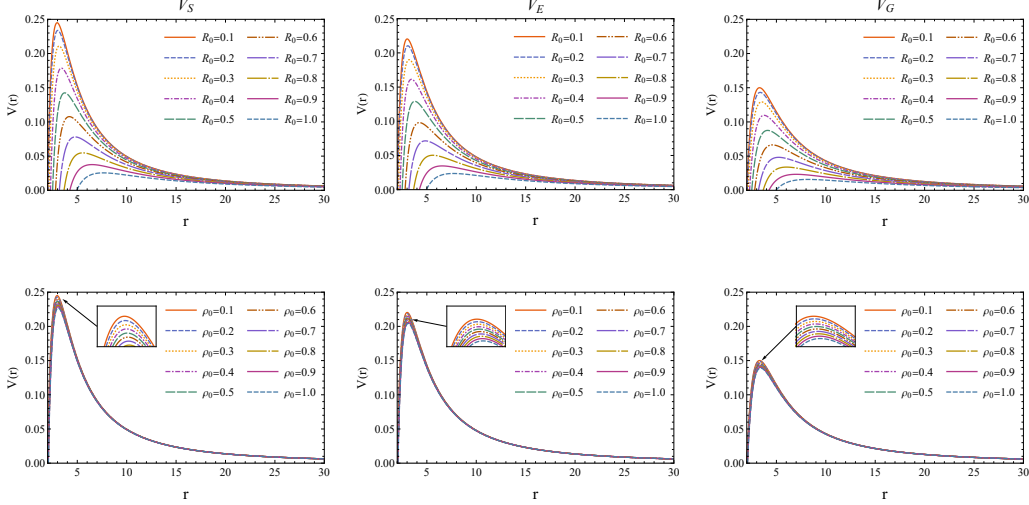


Figure 1: The graphics of  $V_{eff}$  for different perturbed fields  $V_S$  (scalar field),  $V_E$  (electromagnetic field), and  $V_G$  (gravitational field) at  $\ell = 2$ , respectively. The first row is  $V_{eff}$  for changing  $R_0$  at  $\rho_0 = 0.1$ , the second row is  $V_{eff}$  for changing  $\rho_0$  at

$$R_0 = 0.1.$$

Fig. 1 shows graphics of  $V_{eff}$  for three different perturbed fields  $V_S$  ( $s = 0$ ),  $V_E$  ( $s = 1$ ), and  $V_G$  ( $s = 2$ ). One can see that  $V_S$ ,  $V_E$  and  $V_G$  will become smaller as  $R_0$  or  $\rho_0$  increases. And for  $r$  of the peak, thing is opposite. However,  $\rho_0$  has less impact than  $R_0$ .  $V_{eff}$  will decrease when only  $s$  increases. Although the transformation of

$V_{eff}$  with respect to  $\ell$  is not drawn in Fig. 1, it can be directly concluded by analyzing Eq. (8) that  $V_{eff}$  simply increases as  $\ell$  increases.

### III. QUASINORMAL MODES AND WKB METHOD

The region to be studied should be outside the event horizon, that means  $r > r_+$  or  $r_* \in (-\infty, +\infty)$ . The boundary condition for this problem is

$$\Psi \propto \begin{cases} e^{-i\omega r_*}, & r_* \rightarrow -\infty, \\ e^{i\omega r_*}, & r_* \rightarrow +\infty, \end{cases} \quad (11)$$

which is only an ingoing wave at the horizon and only an outgoing wave at infinity.

The WKB method is based on matching of the asymptotic solutions, with the Taylor expansion around the peak of  $V_{eff}$ . By this way, it is possible to relate the ingoing and outgoing amplitudes through the linear transformation. Then, one could obtain  $k^{\text{th}}$  order WKB formula for solving the QNFs

$$\frac{i(\omega^2 - V_0)}{\sqrt{-2V_2}} + \sum_{i=2}^k \Lambda_i = n + \frac{1}{2}, \quad (12)$$

where  $n$  is principal quantum number,  $V_j$  are set as the  $j^{\text{th}}$  derivative with respect to the  $r_*$  at the peak value of the  $V_{eff}$  ( $j \geq 0$ , defining the "0 derivative" as the original, non-differentiated function), and  $\Lambda_i$  are the correction terms depending on  $V_0$  to  $V_{2i}$  [21–24]. One can obtain the change trend of QNFs by simply analyzing 1<sup>st</sup> order WKB equation. When  $V_0$  or  $n$  increases, the real part and imaginary part



of  $\omega^2$  will increase. [25] states that the real parts of QNFs  $\omega_r$  are positive and the imaginary parts of QNFs  $\omega_i$  are negative, so it can be concluded that  $|\omega_r|$  and  $|\omega_i|$  both increase as  $V_{eff}$  or  $n$  increases, and the increment of  $|\omega_r|$  is greater than that of  $|\omega_i|$ .

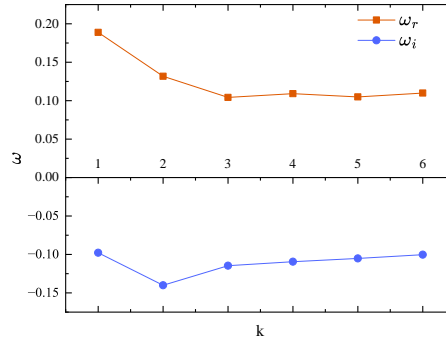


Figure 2:  $\omega_r$  and  $\omega_i$  obtained from  $k^{\text{th}}$  order WKB method. We set  $R_0 = 0.1$ ,

$$\rho_0 = 0.1 \text{ and } \ell = s = n = 0.$$

The WKB method is a method to solve the approximate value, and there is a small error between the obtained result and the exact solution. In Fig. 2, one can observe that the results of the first few orders fluctuate greatly, but the results of the 6<sup>th</sup> order WKB method are not much different from those of 4<sup>th</sup> or 5<sup>th</sup> order WKB method, so the 6<sup>th</sup> order WKB method is chosen for subsequent calculation.

Fig. 3 shows

- as  $R_0$  or  $\rho_0$  increases, the absolute values of both  $|\omega_r|$  and  $|\omega_i|$  of QNFs decrease,

$\rho_0$  has less impact than  $R_0$ ,

- both  $|\omega_r|$  and  $|\omega_i|$  decrease as  $s$  increases,
- the increment of  $|\omega_r|$  is greater than that of  $|\omega_i|$ .

Fig. 3 agrees with our previous analyses. From these one can conclude that as  $\ell$  or  $n$  increases,  $|\omega_r|$  and  $|\omega_i|$  increase.

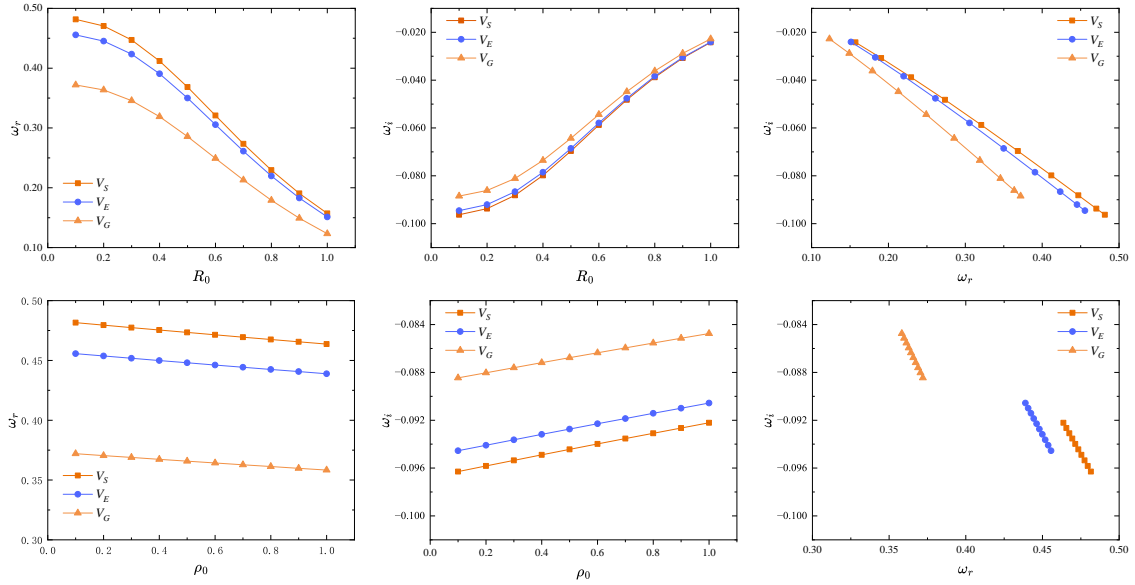


Figure 3: The QNFs for different perturbed fields at  $\ell = 2$  and  $n = 0$ . The first row plots are  $V_{eff}$  for changing  $R_0$  at  $\rho_0 = 0.1$ , the second row plots are  $V_{eff}$  for changing  $\rho_0$  at  $R_0 = 0.1$ .

#### IV. QUASINORMAL MODES AND THE PHOTON SPHERE RADIUS

QNMs, as a gravitational wave propagating through the spacetime created by the black hole, should have some relationship with other properties of the black hole. There is a close connection between null geodesics and QNMs. In the eikonal limit, the relationship between QNFs and null geodesics of black holes is given by [? ],

$$\omega = \lim_{\ell \gg 1} \left( \Omega \ell - i \left( n + \frac{1}{2} \right) \lambda \right), \quad (13)$$

$$\Omega = \frac{\sqrt{f'(r_{ps})}}{r_{ps}}, \quad (14)$$

$$\lambda = \sqrt{\frac{f(r_{ps}) [2f(r_{ps}) - r^2 f''(r_{ps})]}{2r_{ps}^2}}, \quad (15)$$

where  $\Omega$  is the angular velocity at the null geodesic orbit,  $\lambda$  is the Lyapunov exponent that determines the instability time scale of the orbit, and  $r_{ps}$  is the photon sphere radius solved by  $d(f(r)/r^2)/dr = 0$ .  $f'(r)$  and  $f''(r)$  represent the first and second derivatives of  $f(r)$  to  $r$ , respectively. The previous analyses of the variation of  $|\omega_r|$  or  $|\omega_i|$  with  $\ell$  and  $n$  agrees with Eq. (13).

Through the analysis of Table I and II, it could be seen that increasing  $s$  will reduce the deviation of  $\omega_r$ , but it will amplify the deviation of  $\omega_i$ . For a fixed  $s$ , with the increase of  $\ell$ , the deviations caused by two methods for  $\omega_r$  and  $\omega_i$  both gradually decreases to an acceptable extent. But it's worth noting that to obtain a same deviation range, the value of  $\ell$  that  $\omega_i$  need is smaller compared with  $\omega_r$ .

Table I: The relative deviation of  $\omega_r$  of the WKB method and the eikonal limit formula when  $n = 0$ ,  $\rho_0 = 0.1$  and  $R_0 = 0.1$ .

|         | $\ell = 2$ | $\ell = 3$ | $\ell = 4$ | $\ell = 5$ | $\ell = 10$ | $\ell = 100$ | $\ell = 10^3$ | $\ell = 10^4$ | $\ell = 10^5$ |
|---------|------------|------------|------------|------------|-------------|--------------|---------------|---------------|---------------|
| $s = 0$ | 20.416%    | 14.513%    | 11.253%    | 9.188%     | 4.790%      | 0.498%       | 0.050%        | 0.005%        | 0.001%        |
| $s = 1$ | 15.889%    | 12.111%    | 9.765%     | 8.175%     | 4.501%      | 0.495%       | 0.050%        | 0.005%        | 0.001%        |
| $s = 2$ | 3.0159%    | 3.687%     | 4.868%     | 4.944%     | 3.620%      | 0.485%       | 0.050%        | 0.005%        | 0.001%        |

Table II: The relative deviation of  $\omega_i$  of the settlement result of the WKB method and the eikonal limit formula when  $n = 0$ ,  $\rho_0 = 0.1$  and  $R_0 = 0.1$ .

|         | $\ell = 2$ | $\ell = 3$ | $\ell = 4$ | $\ell = 5$ | $\ell = 10$ | $\ell = 100$      | $\ell = 10^3$     |
|---------|------------|------------|------------|------------|-------------|-------------------|-------------------|
| $s = 0$ | 0.558%     | 0.285%     | 0.173%     | 0.116%     | 0.032%      | $3.4 * 10^{-4}\%$ | $3.5 * 10^{-6}\%$ |
| $s = 1$ | 1.276%     | 0.635%     | 0.380%     | 0.253%     | 0.069%      | $7.5 * 10^{-4}\%$ | $7.6 * 10^{-6}\%$ |
| $s = 2$ | 8.246%     | 3.797%     | 2.187%     | 1.427%     | 0.376%      | 0.004%            | $4.1 * 10^{-5}\%$ |

When  $\ell = 10^3$ , the deviation of  $\omega_i$  is acceptable enough. So we choose  $\ell = 10^3$  to plot Table III to show the deviation of  $\omega_i$  with respect to  $n$ . Table clearly shown that the deviation of two methods is small enough. And generally, deviation will increase with the increase of  $n$ . It can be predictable that one could use a larger  $\ell$  to satisfy eikonal limit more precisely.

Table III: The relative deviation of  $\omega_i$  of the WKB method and the eikonal limit formula when  $\ell = 10^3$ ,  $\rho_0 = 0.1$  and  $R_0 = 0.1$ .

|         | $n = 0$           | $n = 1$           | $n = 2$           | $n = 3$           | $n = 4$           | $n = 5$           |
|---------|-------------------|-------------------|-------------------|-------------------|-------------------|-------------------|
| $s = 0$ | $3.5 * 10^{-6}\%$ | $1.6 * 10^{-5}\%$ | $4.0 * 10^{-5}\%$ | $7.6 * 10^{-5}\%$ | $1.3 * 10^{-4}\%$ | $1.8 * 10^{-4}\%$ |
| $s = 1$ | $7.6 * 10^{-6}\%$ | $4.5 * 10^{-6}\%$ | $2.9 * 10^{-5}\%$ | $6.5 * 10^{-5}\%$ | $1.1 * 10^{-4}\%$ | $1.7 * 10^{-4}\%$ |
| $s = 2$ | $4.1 * 10^{-5}\%$ | $2.9 * 10^{-5}\%$ | $4.7 * 10^{-6}\%$ | $3.2 * 10^{-5}\%$ | $8.0 * 10^{-5}\%$ | $1.4 * 10^{-4}\%$ |

## V. THE WKB METHOD AND GREYBODY FACTOR

Just as tunneling is considered in quantum mechanics, the reflection and transmission of waves through black hole spacetime should also be calculated. There are both ingoing wave and outgoing wave at infinity, but only ingoing wave at horizon. Thus, the boundary condition should be written as

$$\Psi = \begin{cases} T e^{-i\omega r_*}, & r_* \rightarrow -\infty, \\ e^{-i\omega r_*} + R e^{i\omega r_*}, & r_* \rightarrow +\infty, \end{cases} \quad (16)$$

where  $R$  and  $T$  represent the reflection coefficient and transmission coefficient, respectively. The greybody factor is defined as the probability of an outgoing wave reaching to infinity or an incoming wave to be absorbed by the black hole [31–33], so  $|T|^2$  is called the greybody factor.  $R$  and  $T$  should satisfy the following relation

$$|R|^2 + |T|^2 = 1. \quad (17)$$

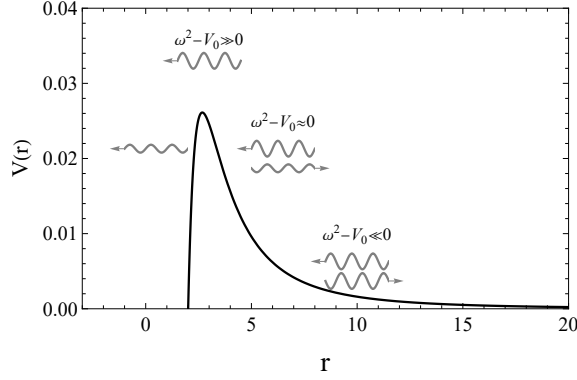


Figure 4: Classification of gravitational wave transmission scenarios.

Table IV: The relationship between the result of  $\omega^2 - V_0$  and whether the reflection or transmission effect is significant.  $\checkmark$  means the transmission effect is obvious,

$\times$  means it is not obvious.

|                            | reflection transmission |              |
|----------------------------|-------------------------|--------------|
| $\omega^2 - V_0 \ll 0$     | $\checkmark$            | $\times$     |
| $\omega^2 - V_0 \approx 0$ | $\checkmark$            | $\checkmark$ |
| $\omega^2 - V_0 \gg 0$     | $\times$                | $\checkmark$ |

Fig. 4 and Table IV show that when  $\omega^2 - V_0 \approx 0$ , the transmission effect and reflection effect are more obvious. This is obviously a condition that satisfies the solution of the WKB method. Using 6<sup>th</sup> order WKB method [40], the reflection and

transmission coefficients could be obtained

$$|R|^2 = \frac{1}{1 + e^{-i2\pi K}}, \quad (18)$$

$$|T|^2 = \frac{1}{1 + e^{+i2\pi K}}, \quad (19)$$

$$K = \frac{i(\omega^2 - V_0)}{\sqrt{-2V_2}} + \sum_{i=2}^6 \Lambda_i, \quad (20)$$

where  $K$  is a parameter obtained by the WKB formula and  $\Lambda_i$  are all imaginary numbers.

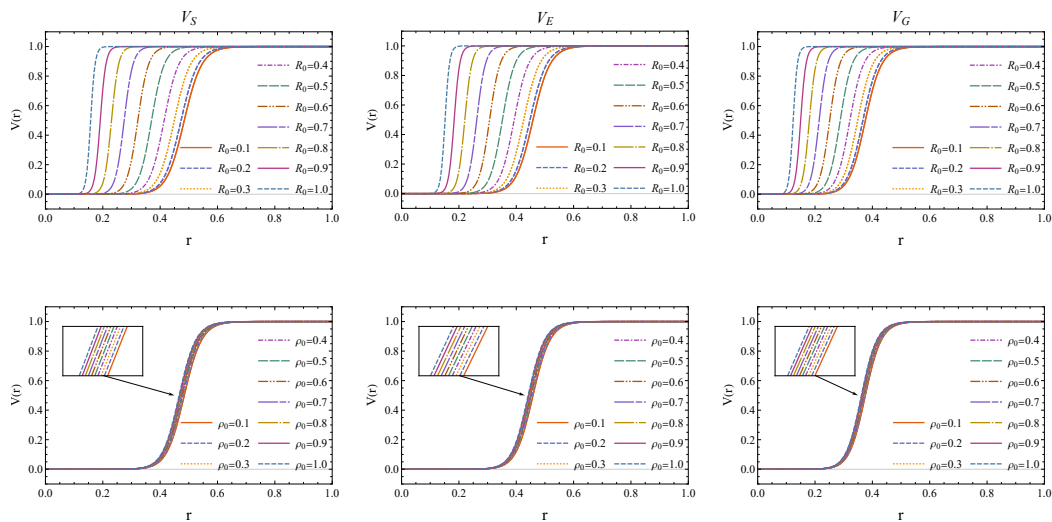


Figure 5: The graphics of  $|T|^2$  for different perturbed fields at  $\ell = 2$ . The first row plots are  $|T|^2$  for changing  $R_0$  at  $\rho_0 = 0.1$ , the second row plots are  $|T|^2$  for changing  $\rho_0$  at  $R_0 = 0.1$ .

From Fig. 5, one can see that  $\omega$  decreases as  $R_0$  or  $\rho_0$  increases at the same

$|T|^2$ , and the effect of  $R_0$  is more obvious than that of  $\rho_0$ . This is consistent with the effective potential, where the height of the potential barrier decrease and the perturbation passes through the potential barrier more easily as  $R_0$  or  $\rho_0$  increases.

## VI. CONCLUSION

In this paper, we studied the perturbation equations of three kinds of perturbation fields with different spins in the background of the Schwarzschild black hole in the CDM halo. The effective potential is calculated and plotted. According to this, it is concluded that with the increase of the dark matter parameter  $R_0$  or  $\rho_0$ , the peak value of the effective potential becomes smaller, and the influence of  $R_0$  is greater. After applying the boundary condition, we calculated QNFs using 6<sup>th</sup> order WKB method. The results shown that both the real parts and the absolut value of the imaginary parts of the QNFs increase as  $R_0$  or  $\rho_0$  decreases. Then the results of the WKB method and the eikonal limit formula are compared, showing the results of the WKB approximation closely match the eikonal limit formula. Finally, we also discussed the greybody factor for these three perturbed fields by used 6<sup>th</sup> order WKB method. The greybody factor increases as  $R_0$  or  $\rho_0$  increases. This is consistent with the effective potential.



## REFERENCES

---

- [1] Albert Einstein. Die feldgleichungen der gravitation. *Sitzung der physikalisch-mathematischen Klasse*, 25:844–847, 1915.
- [2] Albert Einstein. Näherungsweise integration der feldgleichungen der gravitation. *Sitzungsberichte der Königlich Preussischen Akademie der Wissenschaften*, pages 688–696, 1916.
- [3] Albert Einstein. Kosmologische betrachtungen zur allgemeinen relativitätstheorie. *Sitzungsberichte der Königlich Preussischen Akademie der Wissenschaften*, pages 142–152, 1917.
- [4] Hans C Ohanian and Remo Ruffini. *Gravitation and spacetime*. Cambridge University Press, 2013.
- [5] Seven-Year Wilson Microwave Anisotropy Probe. Observations: Sky maps, systematic errors, and basic results. nasa. gov. Technical report, Retrieved 2010-12-02.
- [6] Sean M Carroll. *Dark Matter, Dark Energy: The Dark Side of the Universe. Parts 1 & 2*. Teaching Company, 2007.
- [7] Fritz Zwicky. Die rotverschiebung von extragalaktischen nebeln. *Helvetica physica acta*, 6:110–127, 1933.

- [8] PJE Peebles. Large-scale background temperature and mass fluctuations due to scale-invariant primeval perturbations. *Astrophysical Journal, Letters to the Editor*, 263(1):L1–L5, 1982.
- [9] John Michael Kovac, EM Leitch, Clement Pryke, JE Carlstrom, NW Halverson, and WL Holzzapfel. Detection of polarization in the cosmic microwave background using *dasi*. *Nature*, 420(6917):772–787, 2002.
- [10] Peter AR Ade, N Aghanim, M Arnaud, Mark Ashdown, J Aumont, C Baccigalupi, AJ Banday, RB Barreiro, JG Bartlett, N Bartolo, et al. Planck 2015 results-xiii. cosmological parameters. *Astronomy & Astrophysics*, 594:A13, 2016.
- [11] Zhaoyi Xu, Xian Hou, Xiaobo Gong, and Jiancheng Wang. Black hole space-time in dark matter halo. *Journal of Cosmology and Astroparticle Physics*, 2018(09):038, 2018.
- [12] Shi-Jie Ma, Tian-Chi Ma, Jian-Bo Deng, and Xian-Ru Hu. Shadow of schwarzschild black hole in the cold dark matter halo. *Modern Physics Letters A*, 38(24n25):2350104, 2023.
- [13] Lei You, Rui-bo Wang, Shi-Jie Ma, Jian-Bo Deng, and Xian-Ru Hu. Optical properties of euler-heisenberg black hole in the cold dark matter halo. *arXiv preprint arXiv:2403.12840*, 2024.

- [14] Emanuele Berti, Vitor Cardoso, Jose A Gonzalez, and Ulrich Sperhake. Mining information from binary black hole mergers: a comparison of estimation methods for complex exponentials in noise. *Physical Review D*, 75(12):124017, 2007.
- [15] Fernando Echeverria. Gravitational-wave measurements of the mass and angular momentum of a black hole. *Physical Review D*, 40(10):3194, 1989.
- [16] Emanuele Berti, Vitor Cardoso, and Clifford M Will. Gravitational-wave spectroscopy of massive black holes with the space interferometer lisa. *Physical Review D*, 73(6):064030, 2006.
- [17] Emanuele Berti, Jaime Cardoso, Vitor Cardoso, and Marco Cavaglia. Matched filtering and parameter estimation of ringdown waveforms. *Physical Review D*, 76(10):104044, 2007.
- [18] Maximiliano Isi, Matthew Giesler, Will M Farr, Mark A Scheel, and Saul A Teukolsky. Testing the no-hair theorem with gw150914. *Physical Review Letters*, 123(11):111102, 2019.
- [19] Edward W Leaver. An analytic representation for the quasi-normal modes of kerr black holes. *Proceedings of the Royal Society of London. A. Mathematical and Physical Sciences*, 402(1823):285–298, 1985.
- [20] Paolo Pani. Advanced methods in black-hole perturbation theory. *International Journal of Modern Physics A*, 28(22n23):1340018, 2013.

- [21] Bernard F Schutz and Clifford M Will. Black hole normal modes: a semianalytic approach. *The Astrophysical Journal*, 291:L33–L36, 1985.
- [22] Sai Iyer and Clifford M Will. Black-hole normal modes: A wkb approach. i. foundations and application of a higher-order wkb analysis of potential-barrier scattering. *Physical Review D*, 35(12):3621, 1987.
- [23] RA Konoplya. Quasinormal behavior of the d-dimensional schwarzschild black hole and the higher order wkb approach. *Physical Review D*, 68(2):024018, 2003.
- [24] Jerzy Matyjasek and Michał Opala. Quasinormal modes of black holes: The improved semianalytic approach. *Physical Review D*, 96(2):024011, 2017.
- [25] Bobir Toshmatov, Ahmadjon Abdujabbarov, Zdeněk Stuchlík, and Bobomurat Ahmedov. Quasinormal modes of test fields around regular black holes. *Physical Review D*, 91(8):083008, 2015.
- [26] Tian-Tian Liu, He-Xu Zhang, Yu-Hang Feng, Jian-Bo Deng, and Xian-Ru Hu. Double shadow of a 4d einstein–gauss–bonnet black hole and the connection between them with quasinormal modes. *Modern Physics Letters A*, 37(24):2250154, 2022.
- [27] Vitor Cardoso, Alex S Miranda, Emanuele Berti, Helvi Witek, and Vilson T Zanchin. Geodesic stability, lyapunov exponents, and quasinormal modes. *Physical Review D*, 79(6):064016, 2009.

- [28] Kimet Jusufi. Connection between the shadow radius and quasinormal modes in rotating spacetimes. *Physical Review D*, 101(12):124063, 2020.
- [29] Huan Yang. Relating black hole shadow to quasinormal modes for rotating black holes. *Physical Review D*, 103(8):084010, 2021.
- [30] Davide Pedrotti and Sunny Vagnozzi. See the lightning, hear the thunder: quasinormal modes-shadow correspondence for rotating regular black holes. *arXiv preprint arXiv:2404.07589*, 2024.
- [31] RA Konoplya and AF Zinhailo. Hawking radiation of non-schwarzschild black holes in higher derivative gravity: a crucial role of grey-body factors. *Physical Review D*, 99(10):104060, 2019.
- [32] Vitor Cardoso, Marco Cavaglia, and Leonardo Gualtieri. Black hole particle emission in higher-dimensional spacetimes. *Physical review letters*, 96(7):071301, 2006.
- [33] Sahel Dey and Sayan Chakrabarti. A note on electromagnetic and gravitational perturbations of the bardeen de sitter black hole: quasinormal modes and greybody factors. *The European Physical Journal C*, 79(6):504, 2019.
- [34] Panagiota Kanti and John March-Russell. Calculable corrections to brane black hole decay: The scalar case. *Physical Review D*, 66(2):024023, 2002.
- [35] Stephen W Hawking. Particle creation by black holes. *Communications in mathematical physics*, 43(3):199–220, 1975.

- [36] Naritaka Oshita. Greybody factors imprinted on black hole ringdowns: An alternative to superposed quasinormal modes. *Physical Review D*, 109(10):104028, 2024.
- [37] Tullio Regge and John A Wheeler. Stability of a schwarzschild singularity. *Physical Review*, 108(4):1063, 1957.
- [38] AJM Medved, Damien Martin, and Matt Visser. Dirty black holes: quasinormal modes for ‘squeezed’horizons. *Classical and Quantum Gravity*, 21(9):2393, 2004.
- [39] Hidefumi Nomura and Takashi Tamaki. Continuous area spectrum of a regular black hole. *Physical Review D*, 71(12):124033, 2005.
- [40] RA Konoplya, A Zhidenko, and AF Zinhailo. Higher order wkb formula for quasinormal modes and grey-body factors: recipes for quick and accurate calculations. *Classical and Quantum Gravity*, 36(15):155002, 2019.